Reporting a Misunderstanding in Definition of Functionally Graded Porosity

S.K. Jalali [a*], M.J. Beigrezaee [a], Nicola M. Pugno [a,b*]

[a] Laboratory of Bio-Inspired, Bionic, Nano, Meta Materials & Mechanics, Department of Civil, Environmental and Mechanical Engineering, Università di Trento, via Mesiano, 77, I-38123 Trento, Italy

[b] School of Engineering and Material Science, Queen Mary University of London, Mile End Road, E1 4NS London, United Kingdom

* Corresponding author: nicola.pugno@unitn.it, seyedkamal.jalali@unitn.it

Abstract

This paper reports a misunderstanding in relating Young's modulus to density of functionally graded porous structural members through the well-known power law. A list of recently published references which are subjected to this is presented. It is found out that this misunderstanding may cause undeniable errors in the mechanical responses in both static and dynamic loading conditions that here we quantified by implementing finite element analysis.

Keywords: Porous materials; Functionally Graded Porosity; Open-Cell porosity; Beams, Plates and Shells.

1. Introduction

In the last decades, the field of solid mechanics has been faced a huge variety of modern human-made materials and consequently, many researchers and designers focused to understand how these materials can be implemented to enhance the performance of structural members in new demanded loading situations. Among them fiber-reinforced composites [1] and functionally graded materials [2], especially metal-ceramic combination, attracted one of the most attention. The former was selected as the main candidate for the purpose of light-weight design and the latter was developed to solve challenges in high temperature conditions. Cellular solids [3], also known as porous materials, despite of their remarkable potential in optimizing both functionality and light-weighing were neglected for some decades from a structural point of view. However, thanks to unprecedented developments in manufacturing processes, especially digital manufacturing, they are becoming important alternatives in structural design and parallelly the number of studies on their structural behavior are growing.

Recently, the idea of graded porosity, is introduced to maximize the capability of cellular solids in terms of optimized design for structural members like beams, plates, panels, and shells under a variety of loading conditions [4–6]. Unlike uniform cellular solids, for graded porous ones the amount of porosity is varied as a function of position generally in three dimensions, classifying them as non-homogeneous materials. The present paper is organized to report a misunderstanding widely observed in the recent literature for defining graded porosity and it is clarified how much it may affect the accuracy of obtained results.

2. Explaining the misunderstanding in graded porosity

Consider a bulk material of density ρ_0, Young's modulus E_0, and Poisson's ratio of ν_0 as the parent material of cellular solid. By introducing pores, the density $\rho(x, y, z)$ in every point within the media can be altered as:

$$\rho(x, y, z) = \rho_0(1 - e_m F(x, y, z)) \tag{1}$$

where (x, y, z) denotes the position, e_m is the porosity parameter, and $0 \leq F(x, y, z) \leq 1$ is the gradual function. The maximum of porosity, e_m, happens where $F(x, y, z)$=1, and its minimum is located where $F(x,y,z)$=0 with no pore. Here, we focus on open-cell cellular solids whose Young's modulus is related to its density through a power law of index n as [3]:

$$E(x,y,z) = E_0\left(\frac{\rho(x,y,z)}{\rho_0}\right)^n = E_0\big(1 - e_m F(x,y,z)\big)^n \tag{2}$$

For the case of uniform distribution of pores, the gradual function is canceled in Eqs. (1) and (2), and the uniform density, $\bar{\rho}$, and uniform Young's modulus, $\bar{E}$, are calculated as:

$$\bar{\rho} = \rho_0(1 - e_m) \tag{3a}$$

$$\bar{E} = E_0(1 - e_m)^n = E_0(1 - e_0) \tag{3b}$$

In Eq. (3b), e_0 directly reflects the fraction of reduction in Young's modulus because of pores and is dependent to the porosity parameter, e_m, as:

$$e_0 = 1 - (1 - e_m)^n \,, e_m = 1 - \sqrt[n]{1 - e_0} \tag{4}$$

The misunderstanding happens if someone mixes up Eqs. (3b), (4) and (2) and evaluates the Young's modulus of graded porosity wrongly as:

$$\hat{E}(x,y,z) = E_0\big(1 - e_0 F(x,y,z)\big) \tag{5}$$

A list of 86 recent references, all assuming n=2, in the literature which wrongly used Eq. (5) instead of Eqs. (2), categorizing in three different structural geometries i.e. beams, plates, and shells under a variety of loading conditions named static loading, vibration, dynamic load, stability, and wave propagation, are presented in Table 1.

3. Estimation of Error

The error (%) in evaluation of Young's modulus in every point of a graded porous material is calculated as:

$$Error\ in\ Young's\ Modulus\ (\%) = \frac{\hat{E}(x,y,z) - E(x,y,z)}{E(x,y,z)} \times 100 \tag{6}$$

The error for uniform distribution of porosity is zero, however, for graded porosity is related to gradual function, $F(z)$, porosity parameter, e_m, and power law index, n. As, all the references listed in Table 1 used the power law index n=2, suggested by [3], the same value is considered in the present report.

To demonstrate a numerical insight to this error, a structural member of thickness h where the porosity varies across its thickness is considered. Note that z axis is set along the thickness of member and its origin locates at the mid-plane. As Fig.1 shows, three general types of porosity variation have been chosen called Pyramid, P-type Sandglass, S-type, and diamond, D-type. For the P-type, maximum and minimum of the porosity locate at the bottom and top surfaces of the member, resulting in an unsymmetrical distribution with respect to the mid-plane. For the D-type, as a symmetric distribution, the minimum of the porosity is at the surfaces while the maximum locates at the mid-plane and the S-type is vice versa.

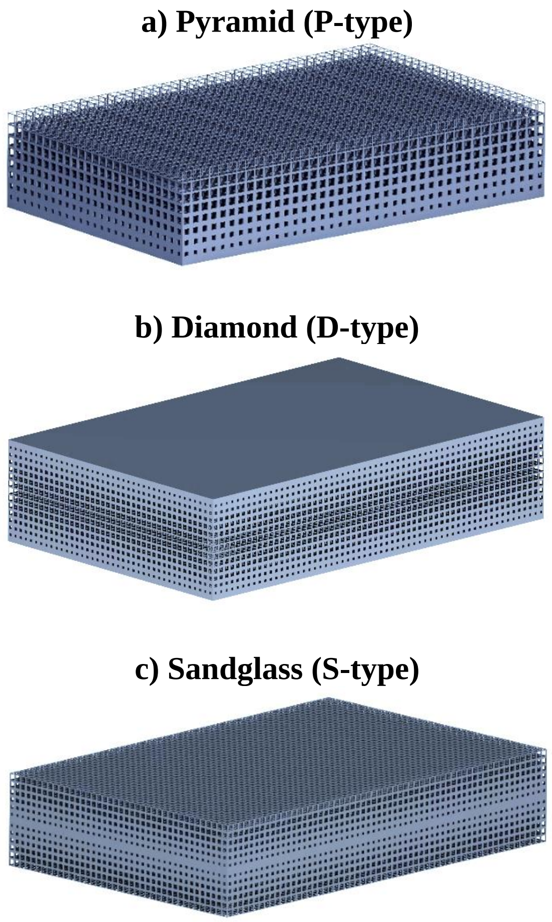

Fig 1. Types of variation of porosity along the thickness a) Pyramid, b) Diamond, and c) Sandglass.

Table 1: A sample list of recent references subjected to the error indicated by Eq. (6).

	Static Load	Vibration	Dynamic Load	Stability	Wave Propagation
Beam	[7] [8] [9] [10] [11] [12]	[7] [13] [14] [15] [16] [17] [18] [19] [8] [20] [9] [21] [22] [23] [24] [25] [10] [26] [27]	[28] [29] [22] [30] [31]	[16] [32] [9] [33] [11] [12]	[34] [35] [36]
Plate	[37] [38] [39] [40]	[41] [37] [42] [43] [44] [45] [46] [47] [48] [49] [50] [51] [52] [53] [54] [55] [56] [57] [58] [59] [60] [61] [62] [63]	[64] [65]	[47] [48] [39] [66]	[67]
Shell	[68] [69] [70]	[71] [72] [73] [74] [75] [76] [77] [78] [79] [80] [81] [82] [83] [84] [85] [86]	[87] [88] [89]	[79] [90] [91]	[92]

Then, four different mathematical functions have been assumed: linear, parabolic, cubic, and cosine. Accordingly, totally 12 definitions for graded function, $F(z)$, are obtained which are listed in Table 2.

Table 2: Definition of gradual function, $F(z)$, across the thickness of structural member.

	P-type	D-type	S-type
[a] Polynomial	$\left(\frac{1}{2}-\frac{z}{h}\right)^m$	$1-\left\lvert\frac{2z}{h}\right\rvert^m$	$\left\lvert\frac{2z}{h}\right\rvert^m$
Cosine	$\cos\left(\frac{\pi z}{2h}+\frac{\pi}{4}\right)$	$\cos\left(\frac{\pi z}{h}\right)$	$\left(1-\cos\left(\frac{\pi z}{h}\right)\right)$

[a] m=1: linear, m =2: parabolic, m =3: cubic

Considering the Cosine function, which is widely addressed by the references in Table 1, Fig. 2 and Fig. 3 depict the variation of error in the calculation of Young's modulus along the thickness for high- and low-range of porosity parameter, e_m, respectively. High range porosity is popular in light-weighting optimal designs, while the low range is usually found in soil mechanics analysis where the porosity hardly exceeds to 0.5. Regardless the value e_m, the error is zero at the surfaces for the P-type, and at the surfaces and mid-plane for the D- and S- types where Eqs. (2) and (5) are equal. Besides, one should notice that for different types of porosity distributions, P-type, D-type, and S-type, the location of maximum value of error shifts with respect to the mid-plane which can affect the rigidity of member significantly.

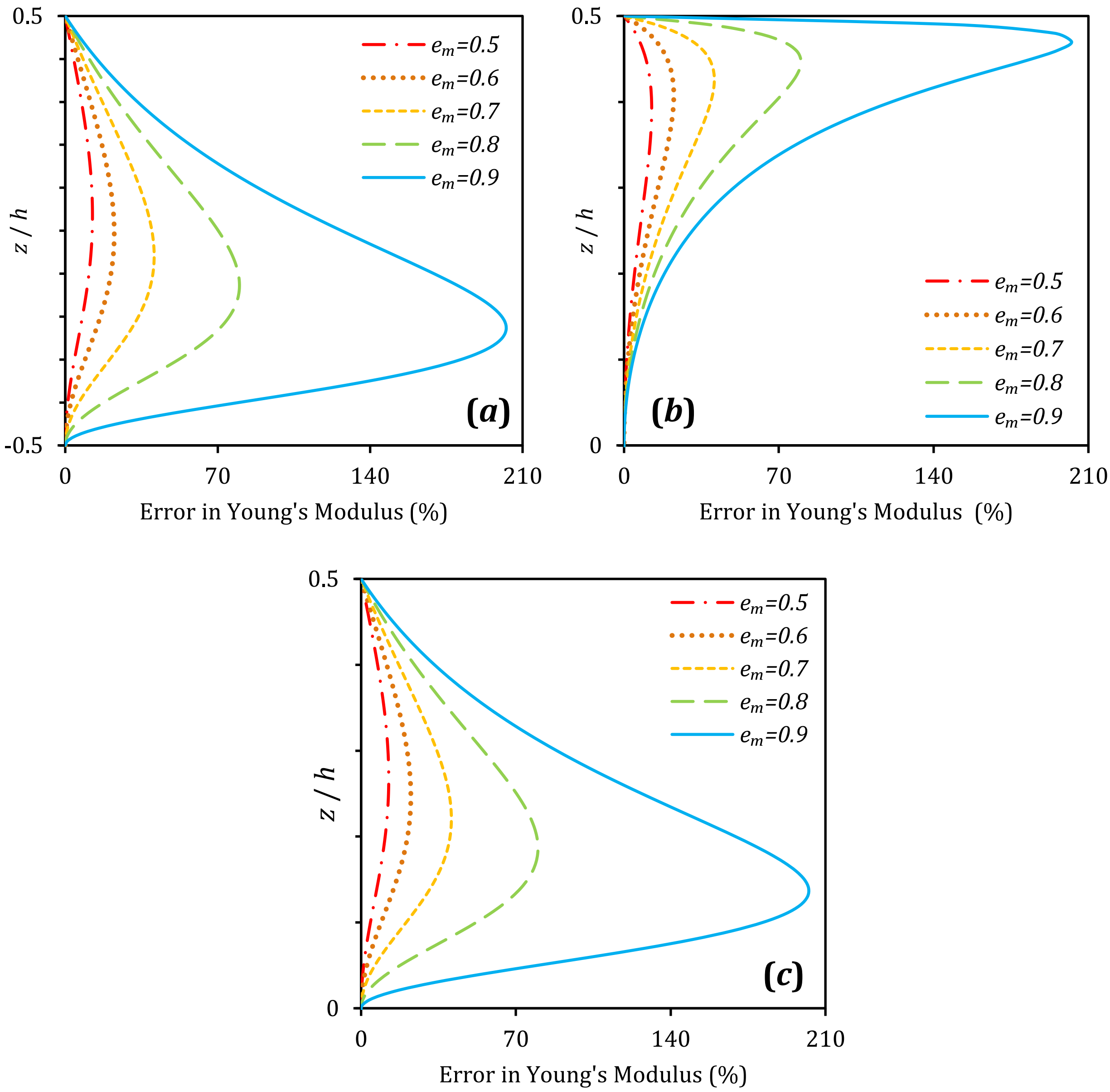

Fig 2. The errors in evaluating Young's modulus via Eq. (5) through the thickness of structural members for cosine distribution and high-range porosity, a) P-type, b) S-type, and c) D-type. The error values for S- and D- types have shown for the half of thickness due to symmetry.

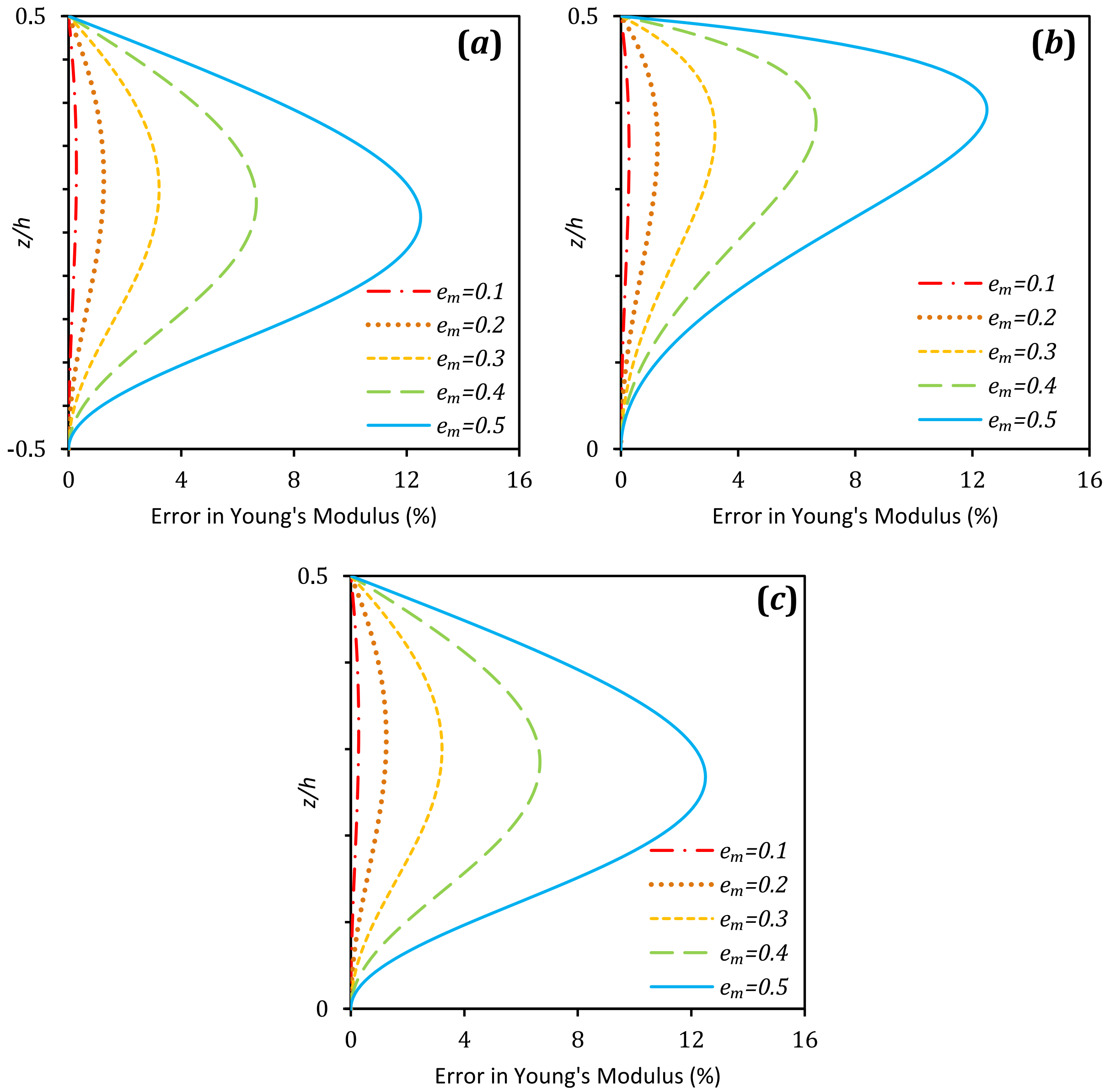

Fig 3. The errors in evaluating Young's modulus via Eq. (5) through the thickness of structural members for cosine distribution and low-range porosity, a) P-type, b) S-type, and c) D-type. The error values for S- and D- types have shown for the half of thickness due to symmetry.

The maximum values of the error for evaluating Young's modulus across the thickness can be calculated by substituting Eqs. (2) and (5) into Eq. (6). After some calculations and simplifications, one can show that the maximum value of error across the thickness is only a function of porosity parameter, e_m, as follows:

$$Maximum\ Error\ in\ Young's\ Modulus\ (\%) = \frac{e_m^2}{4(1-e_m)} \times 100 \tag{7}$$

Interestingly, this maximum is the same for all 12 different porosity graded functions introduced in Table 2, although the location of this maximum is not, as shown in Figs. (2) and (3). The variation of maximum error of Eq. (7) with respect to the porosity parameter, e_m, is plotted in Fig. (4). It is revealed that for a relatively low value of porosity, e_m=0.5, the maximum error is 12.5% while it significantly increases up to 202.5% for a high value of porosity, e_m=0.9. In general, it is concluded that the underlined misunderstanding causes an irrefutable error in the evaluation of Young's modulus for the case of graded porosity along the thickness of structural members. One should pay enough attention that the positive values of error for all cases mean Young's modulus evaluated by Eq. (5) is an overestimation which results in an unreal stiffness for structural members.

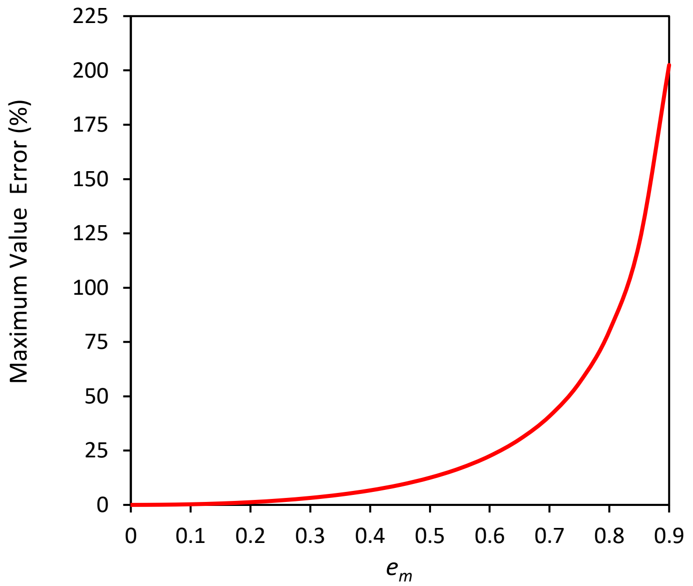

Fig 4. Maximum value of error (%) in evaluation of Young's modulus of graded porosity by Eq. (7).

The next question is how much the reported error in the evaluation of Young's modulus may affect the response of graded porous structural members. Based on the well-known theories of beams, plates, and shells [93], the influence of Young's modulus is reflected in governing equations of structural members as stretching, A, stretching-bending, B, and bending, D, stiffnesses, obtaining by integration across the thickness of members, h, as:

$$(A, \hat{A}) = \int_{-h/2}^{+h/2} \frac{(E, \hat{E})}{1 - \nu_0^2} \, dz \tag{8a}$$

$$(B, \hat{B}) = \int_{-h/2}^{+h/2} \frac{(E, \hat{E})}{1 - \nu_0^2} \, z \, dz \tag{8b}$$

$$(D, \hat{D}) = \int_{-h/2}^{+h/2} \frac{(E, \hat{E})}{1 - \nu_0^2} \, z^2 \, dz \tag{8c}$$

where $\hat{A}$, $\hat{B}$, and $\hat{D}$ are the mistaken stiffnesses using $\hat{E}$ defined by Eq. (5) and ν_0 is the Poisson's ratio of the bulk material which is considered to be constant and is neglected for beam-like members. Due to symmetry, stretching-bending stiffness is zero for S- and D- types. One can calculates the corresponding errors in stiffnesses as:

$$Error\ in\ Stiffness\ (\%) = \frac{(\hat{A}, \hat{B}, \hat{D}) - (A, B, D)}{(A, B, D)} \times 100 \tag{9}$$

It is noted that this error is independent of the thickness of the member and the Poisson's ratio as they are canceled from the fraction.

Fig. 5 shows the error in stiffnesses, A, B, and D because of the reported misunderstanding in the variation of Young's modulus along the thickness of a structural member for the porosity distributions introduced in Table 2. To emphasize the error, the situation where the value of porosity gradually varies across the thickness between 0 to the maximum of 0.99, is considered. Although $e_m = 0.99$ may not practically reachable for uniform porosity, however, it is meaningful for graded porosity as an ideal upper bond. The values of error presented on the top of bars in Fig. 5, show remarkable errors for all graded porosities. For stretching and bending stiffnesses, the errors are positives which means members are considered wrongly stiffer for both in-plane and out-of-plane deformations. Nevertheless, stretching-bending stiffness shows no error for Linear, negative errors for both Parabolic and Cubic, and positive error for Cosine gradual functions. A negative error means the reported misunderstanding underestimates the coupling between in-plane and out-of-plane deformations while positive one overestimates it.

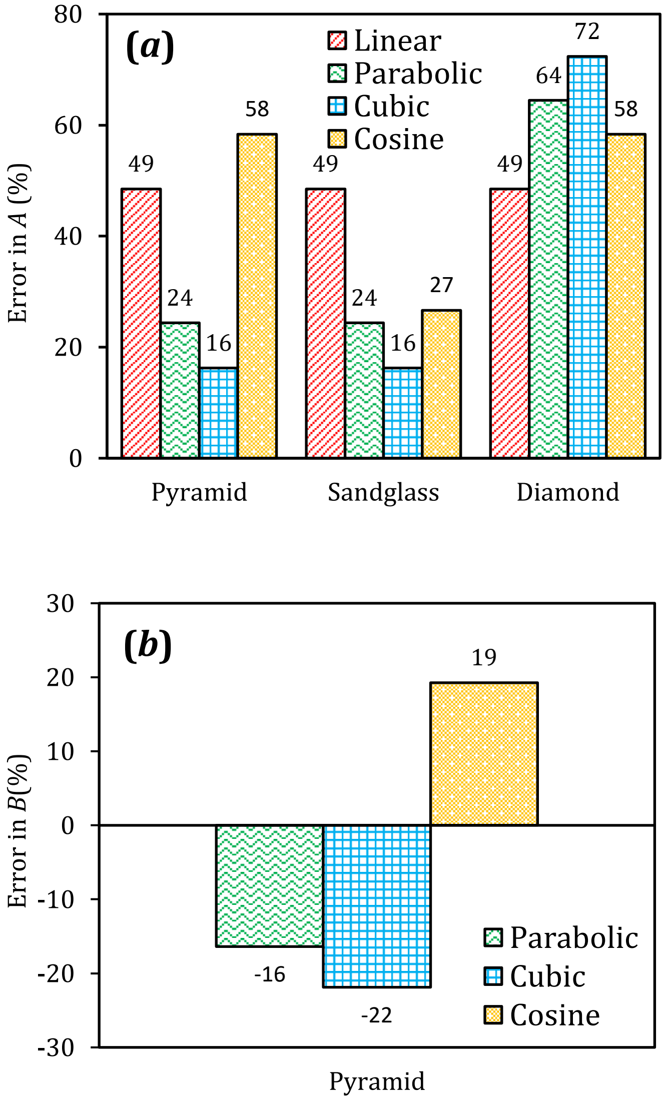

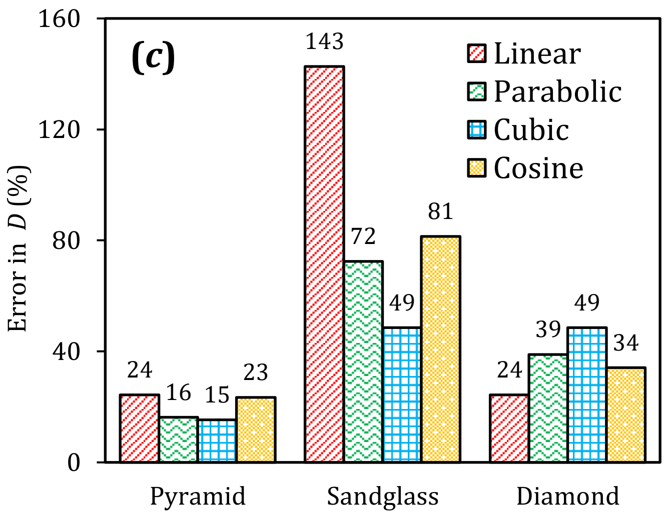

Fig 5. Error in stiffnesses for e_m=0.99. a) Stretching Stiffness, *A*, b) Stretching-Bending Stiffness, *B*, and c) Bending Stiffness, *D*.

The mentioned errors in Eq. (9) and demonstrated in Fig. (5) directly affect the responses of structural members under all static and dynamic loading conditions. For the structural members with low slenderness ratios, usually called thin structures, the relationship between responses and stiffnesses is straightforward. As an example, deflection, w, transverse natural frequencies, ω, and critical buckling load, P_{cr} of a thin member having symmetric material distribution with respect to its mid-plane (S-type and D-type) are simply related to the bending stiffness. Hence, it is possible to find out how much $\hat{w}$, $\hat{\omega}$, and $\hat{P}_{cr}$, predicted based on Eq. (5), are wrong:

$$w \propto \frac{1}{D} \rightarrow w = (\hat{D}/D)\hat{w} \tag{10a}$$

$$\omega \propto \sqrt{D} \rightarrow \omega = \sqrt{D/\hat{D}}\,\hat{\omega} \tag{10b}$$

$$P_{cr} \propto D \rightarrow P_{cr} = \left(D/\hat{D}\right)\hat{P}_{cr} \tag{10c}$$

4. Finite Element Simulation Case studies

To make a better insight to the errors even for thick structural members, bending and free vibration analysis of a square plate with simply supported boundary conditions and graded porosity along its thickness is numerically examined based on the finite element analysis using COMSOL Multiphysics commercial software. To achieve this, a square shell model with the length side of a is modeled and different slenderness ratios are defined by fixing the side length and setting a proper value of thickness, h. The model is meshed by implementing 20 elements through the thickness, and 30×30 in-plane elements, a total of 18000 quadratic elements. The well-known first-order shear deformable theory (FSDT) is implemented to also assure the accuracy of results for thick plates. In the case of bending analysis, a uniform distributed load, q_0, is applied on the surface of the plate. The Poisson's ratio is considered ν_0=0.3. As an isotropic but non-homogeneous material, density is defined as a function along the thickness by Eq. (1) with the bulk value of ρ_0=7800 kg/m^3, while Young's modulus is defined either by Eq. (2) or Eq. (5) considering the bulk value of E_0=200 GPa to calculate the resulting errors in maximum deflections and fundamental natural frequencies for all 12 different porosity distribution functions of Table 2, thanks to the simple functional definition of properties in COMSOL Multiphysics. Finally, stationary and eigenfrequency analyses are performed and the errors are evaluated as follow:

$$Error\ in\ defelction, frequency\ (\%) = \frac{(\widehat{w}, \widehat{\omega}) - (w, \omega)}{(w, \omega)} \times 100 \qquad (11)$$

First, the validation study of the present finite element model is performed. The length side and the thickness are set to a=1000 mm and h=1 mm to model a thin enough plate and a uniform pressure of q_0=1 Pa is applied. Table 3 compares FEM results to those obtained from the exact analytical solution for deflection of thin simply supported square plates in [93] as:

$$w_{max} = 0.00406 \frac{q_0 a^4}{D} \qquad (12)$$

It is noted that the comparison is only possible for symmetric distribution of properties with respect to the mid-plane. In the other word, Eq. (12) is not valid for P-type porosity distribution as stretching-bending stiffness, B, is not zero. An excellent agreement between FEM and exact solution is observed that validate the accuracy of numerical model. Besides, Table 3 reveals remarkable errors in the deflection of thin plates caused by using Eq. (5). It is observed that for S- and D-types where Eq. (10) is valid, the value of error is consistent with the value of error in bending stiffness, D, presented in Fig. 5(c) where the maximum error is for Sandglass-Linear type and the lowest one belongs to Diamond-Linear porosity distribution. The high value of error for Pyramid-Cosine type reflects all the errors in A, B, and D stiffnesses as a stretching-bending coupling happens.

Table 3: Validation of the finite element model by comparing the maximum deflection of thin, porous square plate, w_{max} [mm], to the exact solution of thin plates in Eq. (11) and evaluation of the errors [%] caused by using Eq. (5) instead of Eq. (2). Note: a=1000 mm, h=1 mm, E_0=200 GPa, ν_0=0.3, e_m=0.99, q_0=1 Pa.

Type		h/a=0.001			
		w_{max} [Exact]	w_{max} [FEM]		Error [%]
		Eq. (12)	Eq. (2)	Eq. (5)	Eq. (11)
Sandglass	Linear	2.1509	2.1522	0.8870	-58.7864
	Parabolic	0.9553	0.9559	0.5544	-42.0023
	Cubic	0.6584	0.6588	0.4436	-32.6655
	Cosine	1.1117	1.1124	0.6130	-44.8939
Diamond	Linear	0.3676	0.3678	0.2957	-19.6030
	Parabolic	0.5131	0.5134	0.3697	-27.9899
	Cubic	0.6584	0.6588	0.4436	-32.6655
	Cosine	0.4659	0.4662	0.3475	-25.4612
Pyramid	Linear	-	1.4348	0.6652	-53.6381
	Parabolic	-	0.7553	0.4669	-38.1835
	Cubic	-	0.5655	0.3960	-29.9735
	Cosine	-	3.5867	1.3097	-63.4845

After validation, the values of errors in the deflection and the fundamental frequency of the porous square plates are calculated for various values of slenderness ratio in Table 4 and Table 5, respectively. It is seen that the errors are affected significantly by the types of porosity distribution while they are not much sensitive to the slenderness ratio. It is noted that although the values of deflection and natural frequencies are dependent to the material properties of the bulk, however, for a linear analysis, the values of error are independent as the bulk properties are cancelled in Eq. (11).

One should remember that Eq. (5) overestimates Young's modulus and wrongly considers the plate stiffer. It means using Eq. (5) underestimates and overestimates the deflections and the frequencies, respectively, which justifies the error percentage sign in Table 4 and Table 5.

Table 4: Finite element evaluation of the errors [%] in maximum deflection, w_{max} [mm] of moderately thick, porous square plate caused by using Eq. (5) instead of Eq. (2) for various slenderness ratios. Note: a=1000 mm, h=10, 100, and 200 mm, E_0=200 GPa, ν_0=0.3, e_m=0.99, q_0=1 kPa, 1 MPa, and 10 MPa.

Type		*h/a*=0.01, q_0=1 kPa			*h/a*=0.1, q_0=1 MPa			*h/a*=0.2, q_0=10 MPa		
		Eq. (2)	Eq. (5)	Error [%]	Eq. (2)	Eq. (5)	Error [%]	Eq. (2)	Eq. (5)	Error [%]
Sandglass	Linear	2.1525	0.8872	-58.79	2.1863	0.9099	-58.38	2.8609	1.2236	-57.23
	Parabolic	0.9561	0.5546	-41.99	0.9773	0.5717	-41.51	1.3021	0.7792	-40.16
	Cubic	0.6589	0.4437	-32.66	0.6766	0.4589	-32.18	0.9125	0.6311	-30.85
	Cosine	1.1126	0.6132	-44.89	1.1352	0.6310	-44.41	1.5048	0.8565	-43.08
Diamond	Linear	0.3682	0.2960	-19.61	0.4020	0.3187	-20.71	0.6305	0.4846	-23.14
	Parabolic	0.5140	0.3700	-28.02	0.5701	0.4041	-29.11	0.9252	0.6344	-31.43
	Cubic	0.6596	0.4440	-32.68	0.7380	0.4895	-33.67	1.2196	0.7842	-35.70
	Cosine	0.4667	0.3478	-25.46	0.5162	0.3791	-26.56	0.8331	0.5925	-28.88
Pyramid	Linear	1.4351	0.6654	-53.63	1.4689	0.6882	-53.15	1.9642	0.9464	-51.82
	Parabolic	0.7555	0.4671	-38.18	0.7767	0.4841	-37.67	1.0513	0.6698	-36.29
	Cubic	0.5656	0.3962	-29.96	0.5833	0.4114	-29.48	0.7959	0.5717	-28.17
	Cosine	3.5872	1.3100	-63.481	3.6368	1.3413	-63.12	4.7337	1.7952	-62.08

Table 5: Finite element evaluation of the errors [%] in fundamental natural frequency, ω [Hz] of moderately thick, porous square plate caused by using Eq. (5) instead of Eq. (2) for various slenderness ratios. Note: a=1000 mm, h=10, 100, and 200 mm, E_0=200 GPa, ν_0=0.3, e_m=0.99.

Type		*h/a*=0.01			*h/a*=0.1			*h/a*=0.2		
		Eq. (2)	Eq. (5)	Error [%]	Eq. (2)	Eq. (5)	Error [%]	Eq. (2)	Eq. (5)	Error [%]
Sandglass	Linear	21.745	33.870	55.76	214.75	332.77	54.96	414.61	633.71	52.85
	Parabolic	28.326	37.191	31.30	278.59	364.16	30.72	532.06	687.63	29.24
	Cubic	32.195	39.233	21.86	315.74	383.29	21.39	598.63	719.79	20.24
	Cosine	26.861	36.183	34.71	264.50	354.67	34.09	506.74	671.50	32.51
Diamond	Linear	52.572	58.636	11.54	496.33	557.54	12.33	866.21	987.12	13.96
	Parabolic	54.225	63.911	17.86	506.83	602.12	18.80	868.47	1047.5	20.61
	Cubic	55.003	67.036	21.88	511.21	627.80	22.81	867.49	1080.3	24.53
	Cosine	54.570	63.208	15.83	510.90	596.29	16.71	878.03	1039.9	18.44
Pyramid	Linear	26.63	39.11	46.85	261.41	382.04	46.15	496.85	717.32	44.37
	Parabolic	31.87	40.53	27.18	312.06	395.30	26.67	589.61	739.55	25.43
	Cubic	34.75	41.52	19.49	375.98	421.79	12.18	700.73	782.81	11.71
	Cosine	19.69	32.58	65.48	288.59	405.99	40.68	543.78	756.46	39.11

To investigate the effect of the value of porosity, Fig. 6 and Fig. 7 respectively demonstrate the errors in deflection and the fundamental natural frequency of the simply supported square plate versus variation of porosity parameter, e_m, for all the graded porosity introduced in Table 2. Two slenderness ratios, h/a=0.1 and 0.2 are assumed to see how the errors are correlated to this ratio. As expected, increasing the porosity parameter, e_m, rises the errors and it is observed that the errors have low dependency on the slenderness ratio.

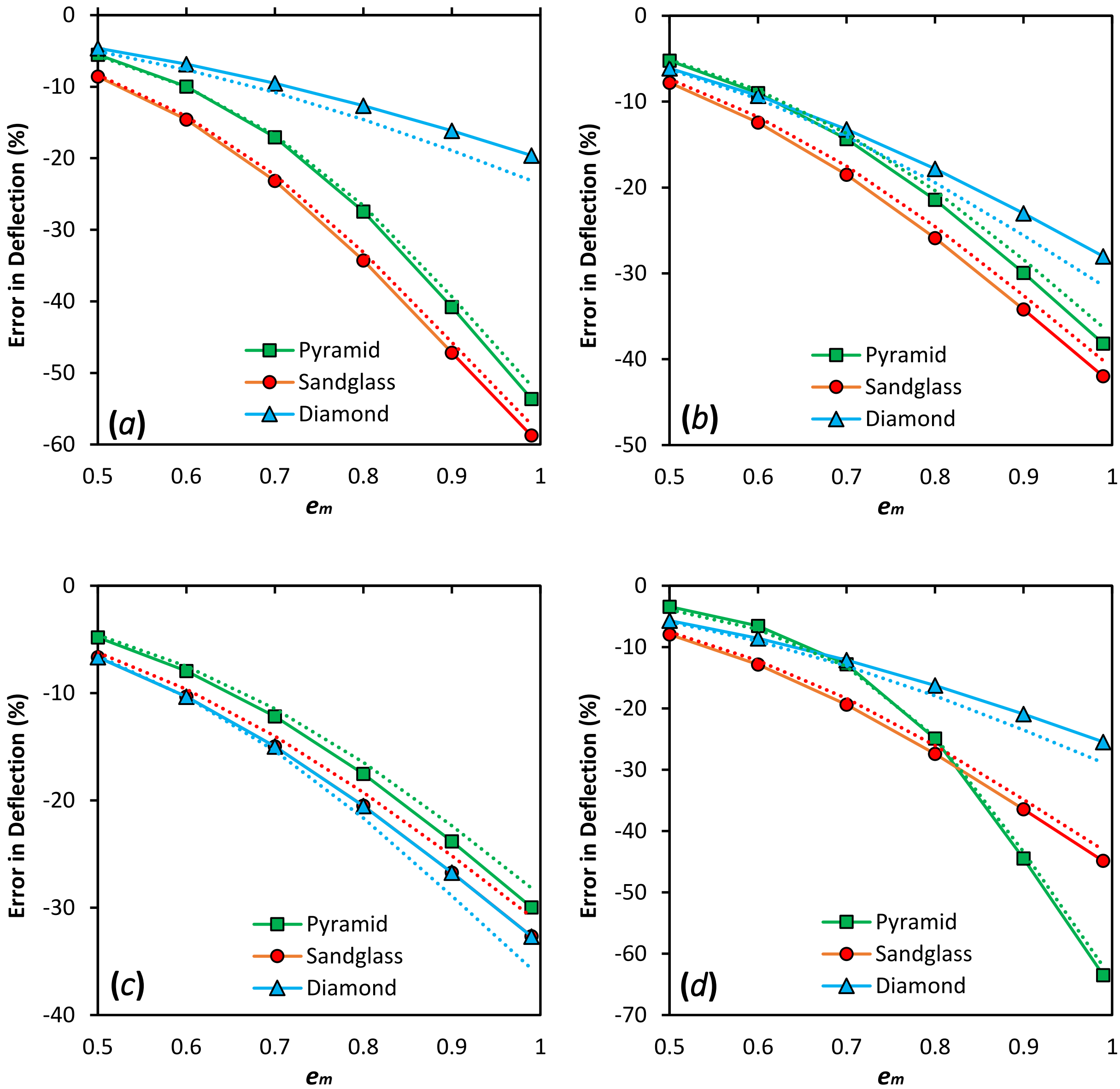

Fig 6. FEM evaluation of the errors in deflection of simply supported square plates with graded porosity. a) Linear, b) Parabolic, c) Cubic, and d) Cosine. Continues lines: h/a=0.01, Dot lines: h/a=0.2.

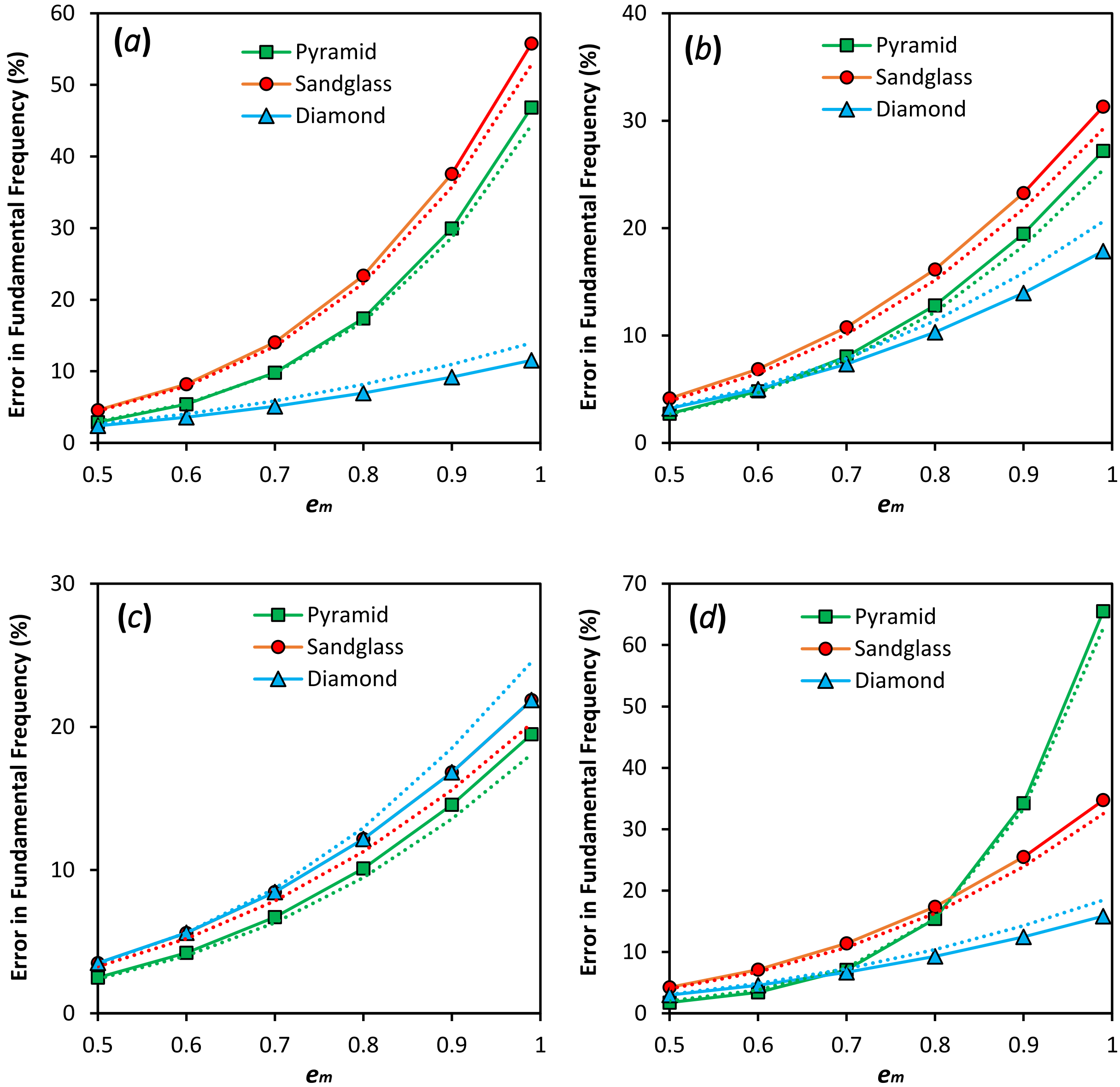

Fig 7. FEM evaluation of the errors in fundamental natural frequency of simply supported square plates with graded porosity. a) Linear, b) Parabolic, c) Cubic, and d) Cosine. Continues lines: h/a=0.01, Dot lines: h/a=0.2.

5. Conclusion

Reviewing the recent literature on beam-, plate-, and shell-like structural members highlights notable attention to the application of modern engineering materials, in particular, the concept of functionally graded porosity due to its advantage in light-weighting optimal designs thanks to remarkable recent developments in digital manufacturing. However, an exhaustive review reveals a misunderstanding in the definition of the graded density-stiffness relationship repeated by many recent publications. The aim of the present paper is to clarify this issue and quantify the value of error that may happen in the evaluation of the stiffness of structural members. Various types of graded porosity distribution across the thickness of structural members are assumed and it is shown that unfortunately, this misunderstanding causes an undeniable stiffness overestimation that significantly affects the predicted behavior of these members in both static and dynamic loading conditions, especially for high values of maximum porosity parameter. As a case study, finite element analysis has been implemented to quantify the value of error in the deflection and frequency response of graded porous square plates.

Acknowledgement

This work was supported by the FET Open (Boheme) grant No. 863179 as well as by Fondazione CARITRO 2018 Laser Surface M., CUP E66C18000800007.

Data Availability

The raw/processed data required to reproduce these findings cannot be shared at this time due to technical or time limitations.

References

[1] Reddy JN, J.N. Reddy. Mechanics of Laminated Composite Plates and Shells Theory and Analysis 2003:840.

[2] Saleh B, Jiang J, Fathi R, Al-hababi T, Xu Q, Wang L, et al. 30 Years of functionally graded materials: An overview of manufacturing methods, Applications and Future Challenges. Composites Part B: Engineering 2020;201:108376. https://doi.org/10.1016/j.compositesb.2020.108376.

[3] Gibson LJ, Ashby MF. Cellular Solids. Cambridge University Press; 1997. https://doi.org/10.1017/CBO9781139878326.

[4] Jalali SK, Heshmati M. Vibration analysis of tapered circular poroelastic plates with radially graded porosity using pseudo-spectral method. Mechanics of Materials 2020;140:103240. https://doi.org/10.1016/j.mechmat.2019.103240.

[5] Heshmati M, Jalali SK. Effect of radially graded porosity on the free vibration behavior of circular and annular sandwich plates. European Journal of Mechanics, A/Solids 2019;74:417–30. https://doi.org/10.1016/j.euromechsol.2018.12.009.

[6] Jalali SK, Beigrezaee MJ, Pugno NM. Is it always worthwhile to resolve the governing equations of plate theories for graded porosity along the thickness? Composite Structures 2020;256:112960. https://doi.org/10.1016/j.compstruct.2020.112960.

[7] Wang YQ, Zhao HL, Ye C, Zu JW. A porous microbeam model for bending and vibration analysis based on the sinusoidal beam theory and modified strain gradient theory. International Journal of Applied Mechanics 2018;10. https://doi.org/10.1142/S175882511850059X.

[8] Fang W, Yu T, Van Lich L, Bui TQ. Analysis of thick porous beams by a quasi-3D theory and isogeometric analysis. Composite Structures 2019;221:110890. https://doi.org/10.1016/j.compstruct.2019.04.062.

[9] Fahsi B, Bouiadjra RB, Mahmoudi A, Benyoucef S, Tounsi A. Assessing the Effects of Porosity on the Bending, Buckling, and Vibrations of Functionally Graded Beams Resting on an Elastic Foundation by Using a New Refined Quasi-3D Theory. Mechanics of Composite Materials 2019;55:219–30. https://doi.org/10.1007/s11029-019-09805-0.

[10] Magnucki K, Witkowski D, Lewiński J. Bending and free vibrations of beams with symmetrically varying mechanical properties—Shear effect. Mechanics of Advanced Materials and Structures 2020;27:325–32. https://doi.org/10.1080/15376494.2018.1472350.

[11] Chen D, Yang J, Kitipornchai S. Elastic buckling and static bending of shear deformable functionally graded porous beam. Composite Structures 2015;133:54–61. https://doi.org/10.1016/j.compstruct.2015.07.052.

[12] Magnucka-Blandzi E. Dynamic Stability and Static Stress State of a Sandwich Beam with a Metal Foam Core Using Three Modified Timoshenko Hypotheses. Mechanics of Advanced Materials and Structures 2011;18:147–58. https://doi.org/10.1080/15376494.2010.496065.

[13] Wattanasakulpong N, Chaikittiratana A, Pornpeerakeat S. Chebyshev collocation approach for vibration analysis of functionally graded porous beams based on third-order shear deformation theory. Acta Mechanica Sinica/Lixue Xuebao 2018;34:1124–35. https://doi.org/10.1007/s10409-018-0770-3.

[14] Wu D, Liu A, Huang Y, Huang Y, Pi Y, Gao W. Dynamic analysis of functionally graded porous structures through finite element analysis. Engineering Structures 2018;165:287–301.

https://doi.org/10.1016/j.engstruct.2018.03.023.

[15] Zhao J, Wang Q, Deng X, Choe K, Xie F, Shuai C. A modified series solution for free vibration analyses of moderately thick functionally graded porous (FGP) deep curved and straight beams. Composites Part B: Engineering 2019;165:155–66. https://doi.org/10.1016/j.compositesb.2018.11.080.

[16] Bamdad M, Mohammadimehr M, Alambeigi K. Analysis of sandwich Timoshenko porous beam with temperature-dependent material properties: Magneto-electro-elastic vibration and buckling solution. JVC/Journal of Vibration and Control 2019;25:2875–93. https://doi.org/10.1177/1077546319860314.

[17] Chen D, Yang J, Kitipornchai S. Free and forced vibrations of shear deformable functionally graded porous beams. International Journal of Mechanical Sciences 2016;108–109:14–22. https://doi.org/10.1016/j.ijmecsci.2016.01.025.

[18] Chen D, Kitipornchai S, Yang J. Nonlinear free vibration of shear deformable sandwich beam with a functionally graded porous core. Thin-Walled Structures 2016;107:39–48. https://doi.org/10.1016/j.tws.2016.05.025.

[19] Qin B, Zhong R, Wang Q, Zhao X. A Jacobi-Ritz approach for FGP beams with arbitrary boundary conditions based on a higher-order shear deformation theory. Composite Structures 2020;247:112435. https://doi.org/10.1016/j.compstruct.2020.112435.

[20] Alasadi AA, Ahmed RA, Faleh NM. Analyzing nonlinear vibrations of metal foam nanobeams with symmetric and non-symmetric porosities. Advances in Aircraft and Spacecraft Science 2019;6:273–82. https://doi.org/10.12989/aas.2019.6.4.273.

[21] Arani AG, Zarei HBA, Pourmousa P. Free Vibration Response of FG Porous Sandwich Micro-Beam with Flexoelectric Face-Sheets Resting on Modified Silica Aerogel Foundation. International Journal of Applied Mechanics 2019;11. https://doi.org/10.1142/S175882511950087X.

[22] Babaei M, Asemi K, Safarpour P. Natural Frequency and Dynamic Analyses of Functionally Graded Saturated Porous Beam Resting on Viscoelastic Foundation Based on Higher Order Beam Theory. Isme 2019;11:615–34. https://doi.org/10.22034/JSM.2019.666691.

[23] Amir S, Soleimani-Javid Z, Arshid E. Size-dependent free vibration of sandwich micro beam with porous core subjected to thermal load based on SSDBT. ZAMM Zeitschrift Fur Angewandte Mathematik Und Mechanik 2019;99:1–21. https://doi.org/10.1002/zamm.201800334.

[24] Ebrahimi F, Dabbagh A. Vibration analysis of graphene oxide powder-/carbon fiber-reinforced multi-scale porous nanocomposite beams: A finite-element study. European Physical Journal Plus 2019;134. https://doi.org/10.1140/epjp/i2019-12594-1.

[25] Heshmati M, Daneshmand F. Vibration analysis of non-uniform porous beams with functionally graded porosity distribution. Proceedings of the Institution of Mechanical Engineers, Part L: Journal of Materials: Design and Applications 2019;233:1678–97. https://doi.org/10.1177/1464420718780902.

[26] Alambeigi K, Mohammadimehr M, Bamdad M, Rabczuk T. Free and forced vibration analysis

of a sandwich beam considering porous core and SMA hybrid composite face layers on Vlasov's foundation. Acta Mechanica 2020. https://doi.org/10.1007/s00707-020-02697-5.

[27] Magnucka-Blandzi E, Magnucki K. Effective design of a sandwich beam with a metal foam core. Thin-Walled Structures 2007;45:432–8. https://doi.org/10.1016/j.tws.2007.03.005.

[28] Chen D, Kitipornchai S, Yang J. Dynamic Response of Shear Deformable Functionally Graded Porous Beams. Applied Mechanics and Materials 2016;846:434–9. https://doi.org/10.4028/www.scientific.net/AMM.846.434.

[29] Gao K, Li R, Yang J. Dynamic characteristics of functionally graded porous beams with interval material properties. Engineering Structures 2019;197:109441. https://doi.org/10.1016/j.engstruct.2019.109441.

[30] Hajmohammad MH, Zarei MS, Kolahchi R, Karami H. Visco-piezoelasticity-zigzag theories for blast response of porous beams covered by graphene platelet-reinforced piezoelectric layers. Journal of Sandwich Structures & Materials 2019:109963621983917. https://doi.org/10.1177/1099636219839175.

[31] Lei YL, Gao K, Wang X, Yang J. Dynamic behaviors of single- and multi-span functionally graded porous beams with flexible boundary constraints. Applied Mathematical Modelling 2020;83:754–76. https://doi.org/10.1016/j.apm.2020.03.017.

[32] Barati MR, Zenkour AM. Investigating post-buckling of geometrically imperfect metal foam nanobeams with symmetric and asymmetric porosity distributions. Composite Structures 2017;182:91–8. https://doi.org/10.1016/j.compstruct.2017.09.008.

[33] Gao K, Huang Q, Kitipornchai S, Yang J. Nonlinear dynamic buckling of functionally graded porous beams. Mechanics of Advanced Materials and Structures 2019;0:1–12. https://doi.org/10.1080/15376494.2019.1567888.

[34] Wang YQ, Liang C, Zu JW. Examining wave propagation characteristics in metal foam beams: Euler–Bernoulli and Timoshenko models. Journal of the Brazilian Society of Mechanical Sciences and Engineering 2018;40. https://doi.org/10.1007/s40430-018-1491-z.

[35] Ebrahimi F, Dabbagh A, Rabczuk T, Tornabene F. Analysis of propagation characteristics of elastic waves in heterogeneous nanobeams employing a new two-step porosity-dependent homogenization scheme. Advances in Nano Research 2019;7:135–43. https://doi.org/10.12989/anr.2019.7.2.135.

[36] Wang YQ, Liang C. Wave propagation characteristics in nanoporous metal foam nanobeams. Results in Physics 2019;12:287–97. https://doi.org/10.1016/j.rinp.2018.11.080.

[37] Ebrahimi F, Habibi S. Deflection and vibration analysis of higher-order shear deformable compositionally graded porous plate. Steel and Composite Structures 2016;20:205–25. https://doi.org/10.12989/scs.2016.20.1.205.

[38] Barati MR. Nonlocal-strain gradient forced vibration analysis of metal foam nanoplates with uniform and graded porosities. Advances in Nano Research 2017;5:393–414. https://doi.org/10.12989/anr.2017.5.4.393.

[39] Magnucka-Blandzi E. Axi-symmetrical deflection and buckling of circular porous-cellular

plate. Thin-Walled Structures 2008;46:333–7. https://doi.org/10.1016/j.tws.2007.06.006.

[40] Ghorbanpour Arani A, Zamani MH. Investigation of electric field effect on size-dependent bending analysis of functionally graded porous shear and normal deformable sandwich nanoplate on silica Aerogel foundation. vol. 21. 2019. https://doi.org/10.1177/1099636217721405.

[41] Rezaei AS, Saidi AR. Application of Carrera Unified Formulation to study the effect of porosity on natural frequencies of thick porous-cellular plates. Composites Part B: Engineering 2016;91:361–70. https://doi.org/10.1016/j.compositesb.2015.12.050.

[42] Mahmoudi A, Bachir-bouiadjra R, Benyoucef S. Influence de la porosité sur la vibration libre des plaques FGM sur fondation élastique. Nature & Technology 2017;17:25–36.

[43] Askari M, Saidi AR, Rezaei AS. On natural frequencies of Levy-type thick porous-cellular plates surrounded by piezoelectric layers. Composite Structures 2017;179:340–54. https://doi.org/10.1016/j.compstruct.2017.07.073.

[44] Heshmati M, Daneshmand F. A study on the vibrational properties of weight-efficient plates made of material with functionally graded porosity. Composite Structures 2018;200:229–38. https://doi.org/10.1016/j.compstruct.2018.05.099.

[45] Askari M, Saidi AR, Rezaei AS. An investigation over the effect of piezoelectricity and porosity distribution on natural frequencies of porous smart plates. Journal of Sandwich Structures and Materials 2018. https://doi.org/10.1177/1099636218791092.

[46] Kamranfard MR, Saidi AR, Naderi A. Analytical solution for vibration and buckling of annular sectorial porous plates under in-plane uniform compressive loading. Proceedings of the Institution of Mechanical Engineers, Part C: Journal of Mechanical Engineering Science 2018;232:2211–28. https://doi.org/10.1177/0954406217716197.

[47] Thang PT, Nguyen-Thoi T, Lee D, Kang J, Lee J. Elastic buckling and free vibration analyses of porous-cellular plates with uniform and non-uniform porosity distributions. Aerospace Science and Technology 2018;79:278–87. https://doi.org/10.1016/j.ast.2018.06.010.

[48] Li Q, Wu D, Chen X, Liu L, Yu Y, Gao W. Nonlinear vibration and dynamic buckling analyses of sandwich functionally graded porous plate with graphene platelet reinforcement resting on Winkler–Pasternak elastic foundation. International Journal of Mechanical Sciences 2018;148:596–610. https://doi.org/10.1016/j.ijmecsci.2018.09.020.

[49] Ghorbanpour Arani A, Zamani MH. Nonlocal Free Vibration Analysis of FG-Porous Shear and Normal Deformable Sandwich Nanoplate with Piezoelectric Face Sheets Resting on Silica Aerogel Foundation. Arabian Journal for Science and Engineering 2018;43:4675–88. https://doi.org/10.1007/s13369-017-3035-8.

[50] Amir S, Bidgoli EMR, Arshid E. Size-dependent vibration analysis of a three-layered porous rectangular nano plate with piezo-electromagnetic face sheets subjected to pre loads based on SSDT. Mechanics of Advanced Materials and Structures 2020;27:605–19. https://doi.org/10.1080/15376494.2018.1487612.

[51] Arefi M, Meskini M. Application of hyperbolic shear deformation theory to free vibration analysis of functionally graded porous plate with piezoelectric face-sheets. Structural

Engineering and Mechanics 2019;71:459–67. https://doi.org/10.12989/sem.2019.71.5.459.

[52] Bemani Khouzestani L, Khorshidvand AR. Axisymmetric free vibration and stress analyses of saturated porous annular plates using generalized differential quadrature method. JVC/Journal of Vibration and Control 2019;25:2799–818. https://doi.org/10.1177/1077546319871132.

[53] Zeng S, Wang BL, Wang KF. Nonlinear vibration of piezoelectric sandwich nanoplates with functionally graded porous core with consideration of flexoelectric effect. Composite Structures 2019;207:340–51. https://doi.org/10.1016/j.compstruct.2018.09.040.

[54] Fenjan RM, Ahmed RA, Alasadi AA, Faleh NM. Nonlocal strain gradient thermal vibration analysis of doublecoupled metal foam plate system with uniform and non-uniform porosities. Coupled Systems Mechanics 2019;8:247–57. https://doi.org/10.12989/csm.2019.8.3.247.

[55] Amir S, Arshid E, Rasti-Alhosseini SMA, Loghman A. Quasi-3D tangential shear deformation theory for size-dependent free vibration analysis of three-layered FG porous micro rectangular plate integrated by nano-composite faces in hygrothermal environment. Journal of Thermal Stresses 2020;43:133–56. https://doi.org/10.1080/01495739.2019.1660601.

[56] Emdadi M, Mohammadimehr M, Navi BR. Free vibration of an annular sandwich plate with CNTRC facesheets and FG porous cores using Ritz method. Advances in Nano Research 2019;7:109–23. https://doi.org/10.12989/anr.2019.7.2.109.

[57] Du Y, Wang S, Sun L, Shan Y. Free vibration of rectangular plates with porosity distributions under complex boundary constraints. Shock and Vibration 2019;2019. https://doi.org/10.1155/2019/6407174.

[58] Zhao J, Wang Q, Deng X, Choe K, Zhong R, Shuai C. Free vibrations of functionally graded porous rectangular plate with uniform elastic boundary conditions. Composites Part B: Engineering 2019;168:106–20. https://doi.org/10.1016/j.compositesb.2018.12.044.

[59] Babaei M, Hajmohammad MH, Asemi K. Natural frequency and dynamic analyses of functionally graded saturated porous annular sector plate and cylindrical panel based on 3D elasticity. Aerospace Science and Technology 2020;96:105524. https://doi.org/10.1016/j.ast.2019.105524.

[60] Ebrahimi F, Dabbagh A, Taheri M. Vibration analysis of porous metal foam plates rested on viscoelastic substrate. Engineering with Computers 2020;0123456789. https://doi.org/10.1007/s00366-020-01031-w.

[61] Chen M, Ye T, Zhang J, Jin G, Zhang Y, Xue Y, et al. Isogeometric three-dimensional vibration of variable thickness parallelogram plates with in-plane functionally graded porous materials. International Journal of Mechanical Sciences 2020;169:105304. https://doi.org/10.1016/j.ijmecsci.2019.105304.

[62] Ebrahimi F, Hosseini SHS. Resonance analysis on nonlinear vibration of piezoelectric/FG porous nanocomposite subjected to moving load. European Physical Journal Plus 2020;135:1–23. https://doi.org/10.1140/epjp/s13360-019-00011-4.

[63] Ebrahimi F, Hosseini SHS. Investigation of flexoelectric effect on nonlinear forced vibration of piezoelectric/functionally graded porous nanocomposite resting on viscoelastic foundation. Journal of Strain Analysis for Engineering Design 2020;55:53–68.

https://doi.org/10.1177/0309324719890868.

[64] Zhao J, Xie F, Wang A, Shuai C, Tang J, Wang Q. Dynamics analysis of functionally graded porous (FGP) circular, annular and sector plates with general elastic restraints. Composites Part B: Engineering 2019;159:20–43. https://doi.org/10.1016/j.compositesb.2018.08.114.

[65] Bahaadini R, Saidi AR, Majidi-Mozafari K. Aeroelastic Flutter Analysis of Thick Porous Plates in Supersonic Flow. International Journal of Applied Mechanics 2019;11. https://doi.org/10.1142/S1758825119500960.

[66] Magnucka-Blandzi E. Non-linear analysis of dynamic stability of metal foam circular plate. Journal of Theoretical and Applied Mechanics 2010;48:207–17.

[67] Hu Z, Zhou K, Chen Y. Sound Radiation Analysis of Functionally Graded Porous Plates with Arbitrary Boundary Conditions and Resting on Elastic Foundation. International Journal of Structural Stability and Dynamics 2020;2050068:1–28. https://doi.org/10.1142/S0219455420500686.

[68] Arefi M, Mohammadi M, Rabczuk T. Effect of characteristics and distribution of porosity on electro-elastic analysis of laminated vessels with piezoelectric face-sheets based on higher-order modeling. Composite Structures 2019;225:111085. https://doi.org/10.1016/j.compstruct.2019.111085.

[69] Mohammadi M, Bamdad M, Alambeigi K, Dimitri R, Tornabene F. Electro-elastic response of cylindrical sandwich pressure vessels with porous core and piezoelectric face-sheets. Composite Structures 2019;225:111119. https://doi.org/10.1016/j.compstruct.2019.111119.

[70] Babaei M, Asemi K. Stress analysis of functionally graded saturated porous rotating thick truncated cone. Mechanics Based Design of Structures and Machines 2020;0:1–28. https://doi.org/10.1080/15397734.2020.1753536.

[71] Wang Y, Xie K, Fu T. Vibration analysis of functionally graded porous shear deformable tubes excited by moving distributed loads. Acta Astronautica 2018;151:603–13. https://doi.org/10.1016/j.actaastro.2018.06.003.

[72] Zhao J, Xie F, Wang A, Shuai C, Tang J, Wang Q. A unified solution for the vibration analysis of functionally graded porous (FGP) shallow shells with general boundary conditions. Composites Part B: Engineering 2019;156:406–24. https://doi.org/10.1016/j.compositesb.2018.08.115.

[73] Daemi H, Eipakchi H. Closed form solution for free vibrations analysis of FGPM thick cylinders employing FSDT under various boundary conditions. Composite Structures 2019;229:111403. https://doi.org/10.1016/j.compstruct.2019.111403.

[74] Ghasemi AR, Meskini M. Free vibration analysis of porous laminated rotating circular cylindrical shells. JVC/Journal of Vibration and Control 2019;25:2494–508. https://doi.org/10.1177/1077546319858227.

[75] Li H, Pang F, Ren Y, Miao X, Ye K. Free vibration characteristics of functionally graded porous spherical shell with general boundary conditions by using first-order shear deformation theory. Thin-Walled Structures 2019;144:106331. https://doi.org/10.1016/j.tws.2019.106331.

[76] Wang YQ, Liu YF, Zu JW. On scale-dependent vibration of circular cylindrical nanoporous metal foam shells. Microsystem Technologies 2019;25:2661–74. https://doi.org/10.1007/s00542-018-4262-y.

[77] Ebrahimi F, Dabbagh A, Rastgoo A. Vibration analysis of porous metal foam shells rested on an elastic substrate. Journal of Strain Analysis for Engineering Design 2019;54:199–208. https://doi.org/10.1177/0309324719852555.

[78] Wang YQ, Ye C, Zu JW. Vibration analysis of circular cylindrical shells made of metal foams under various boundary conditions. International Journal of Mechanics and Materials in Design 2019;15:333–44. https://doi.org/10.1007/s10999-018-9415-8.

[79] Zhang Y, Zhang F. Vibration and buckling of shear deformable functionally graded nanoporous metal foam nanoshells. Nanomaterials 2019;9. https://doi.org/10.3390/nano9020271.

[80] Guan X, Sok K, Wang A, Shuai C, Tang J, Wang Q. A general vibration analysis of functionally graded porous structure elements of revolution with general elastic restraints. Composite Structures 2019;209:277–99. https://doi.org/10.1016/j.compstruct.2018.10.103.

[81] Keleshteri MM, Jelovica J. Nonlinear vibration behavior of functionally graded porous cylindrical panels. Composite Structures 2020;239:112028. https://doi.org/10.1016/j.compstruct.2020.112028.

[82] Heshmati M, Daneshmand F, Amini Y, Adamowski J. Vibration behavior of poroelastic thick curved panels with graded open-cell and saturated closed-cell porosities. European Journal of Mechanics, A/Solids 2019;77:103817. https://doi.org/10.1016/j.euromechsol.2019.103817.

[83] Zhao J, Xie F, Wang A, Shuai C, Tang J, Wang Q. Vibration behavior of the functionally graded porous (FGP) doubly-curved panels and shells of revolution by using a semi-analytical method. Composites Part B: Engineering 2019;157:219–38. https://doi.org/10.1016/j.compositesb.2018.08.087.

[84] Setoodeh AR, Shojaee M, Malekzadeh P. Vibrational behavior of doubly curved smart sandwich shells with FG-CNTRC face sheets and FG porous core. Composites Part B: Engineering 2019;165:798–822. https://doi.org/10.1016/j.compositesb.2019.01.022.

[85] Golmohammadi A, Tarkashvand A, Siahtiry MS. Effects of pores different distributions on vibrational behavior of functionally graded porous cylinder applying Haar wavelet computational technique. Composite Structures 2020;235:111729. https://doi.org/10.1016/j.compstruct.2019.111729.

[86] Askari M, Brusa E, Delprete C. Electromechanical vibration characteristics of porous bimorph and unimorph doubly curved panels. Actuators 2020;9. https://doi.org/10.3390/act9010007.

[87] Faleh NM, Fenjan RM, Ahmed RA. Dynamic analysis of graded small-scale shells with porosity distributions under transverse dynamic loads. European Physical Journal Plus 2018;133. https://doi.org/10.1140/epjp/i2018-12152-5.

[88] Sajad Mirjavadi S, Forsat M, Barati MR, Abdella GM, Mohasel Afshari B, Hamouda AMS, et al. Dynamic response of metal foam FG porous cylindrical micro-shells due to moving loads with strain gradient size-dependency. European Physical Journal Plus 2019;134.

https://doi.org/10.1140/epjp/i2019-12540-3.

[89] Chan DQ, Van Thanh N, Khoa ND, Duc ND. Nonlinear dynamic analysis of piezoelectric functionally graded porous truncated conical panel in thermal environments. Thin-Walled Structures 2020;154:106837. https://doi.org/10.1016/j.tws.2020.106837.

[90] Belica T, Malinowski M, Magnucki K. Dynamic stability of an isotropic metal foam cylindrical shell subjected to external pressure and axial compression. Journal of Applied Mechanics, Transactions ASME 2011;78:1–9. https://doi.org/10.1115/1.4003768.

[91] Toan Thang P, Nguyen-Thoi T, Lee J. Mechanical stability of metal foam cylindrical shells with various porosity distributions. Mechanics of Advanced Materials and Structures 2020;27:295–303. https://doi.org/10.1080/15376494.2018.1472338.

[92] Ebrahimi F, Seyfi A. Studying propagation of wave in metal foam cylindrical shells with graded porosities resting on variable elastic substrate. Engineering with Computers 2020. https://doi.org/10.1007/s00366-020-01069-w.

[93] Reddy JN. Theory and Analysis of Elastic Plates and Shells. Philadelphia, PA: Taylor & Francis; 2006. https://doi.org/10.1201/9780849384165.